

# A robotics platform for automated batch fabrication of high density, microfluidics-based DNA microarrays, with applications to single cell, multiplex assays of secreted proteins

Cite as: Rev. Sci. Instrum. **82**, 094301 (2011); <https://doi.org/10.1063/1.3636077>

Submitted: 11 June 2011 • Accepted: 15 August 2011 • Published Online: 16 September 2011

Habib Ahmad, Alex Sutherland, Young Shik Shin, et al.



View Online



Export Citation

## ARTICLES YOU MAY BE INTERESTED IN

[Protein immobilization techniques for microfluidic assays](#)

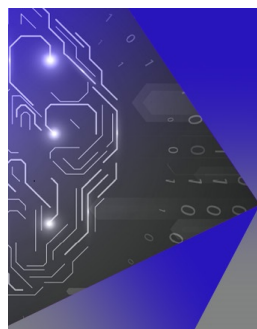
Biomicrofluidics **7**, 041501 (2013); <https://doi.org/10.1063/1.4816934>

[Enhanced single-cell encapsulation in microfluidic devices: From droplet generation to single-cell analysis](#)

Biomicrofluidics **14**, 061508 (2020); <https://doi.org/10.1063/5.0018785>

[A high-throughput cellulase screening system based on droplet microfluidics](#)

Biomicrofluidics **8**, 041102 (2014); <https://doi.org/10.1063/1.4886771>



## APL Machine Learning

Machine Learning for Applied Physics  
Applied Physics for Machine Learning

**First Articles  
Now Online!**

# A robotics platform for automated batch fabrication of high density, microfluidics-based DNA microarrays, with applications to single cell, multiplex assays of secreted proteins

Habib Ahmad, Alex Sutherland, Young Shik Shin, Kiwook Hwang, Lidong Qin,<sup>a)</sup>  
Russell-John Krom, and James R. Heath<sup>b)</sup>

*NanoSystems Biology Cancer Center and Division of Chemistry and Chemical Engineering, California Institute of Technology, MC 127-72, 1200 East California Boulevard, Pasadena, California 91125, USA*

(Received 11 June 2011; accepted 15 August 2011; published online 16 September 2011)

Microfluidics flow-patterning has been utilized for the construction of chip-scale miniaturized DNA and protein barcode arrays. Such arrays have been used for specific clinical and fundamental investigations in which many proteins are assayed from single cells or other small sample sizes. However, flow-patterned arrays are hand-prepared, and so are impractical for broad applications. We describe an integrated robotics/microfluidics platform for the automated preparation of such arrays, and we apply it to the batch fabrication of up to eighteen chips of flow-patterned DNA barcodes. The resulting substrates are comparable in quality with hand-made arrays and exhibit excellent substrate-to-substrate consistency. We demonstrate the utility and reproducibility of robotics-patterned barcodes by utilizing two flow-patterned chips for highly parallel assays of a panel of secreted proteins from single macrophage cells. © 2011 American Institute of Physics. [doi:10.1063/1.3636077]

## I. INTRODUCTION

We describe an integrated robotics/microfluidics platform for automating the molecular printing technique of microfluidics flow-patterning,<sup>1-5</sup> which can be harnessed to produce miniaturized DNA or antibody microarrays. There are multiple patterning techniques that can produce microscopic molecular patterns.<sup>6-10</sup> However, any such technique has tradeoffs that must be balanced against the desired application. These include the degree of multiplexing, the achievable feature shape, size, and pitch, the coverage and spot-to-spot variability of the molecular features, the surface area that can be patterned, and the throughput of the patterning approach. For example, traditional spotted DNA arrays are typically characterized by 150  $\mu\text{m}$  spot sizes, patterned at  $\sim 300 \mu\text{m}$  pitch, and can readily permit a degree of multiplexing of a few hundred. In addition, chip-scale spotted arrays can be produced in moderate throughput, and can yield a high molecular coverage, at high purity, on a given spot. In terms of reproducibility, typical spot-to-spot coverage variation can be from 5%–10% across individual substrates, and 10%–30% between substrates.<sup>11,12</sup> These factors make spotted arrays useful for a host of biological assays; they provide a standard against which other molecular patterning techniques can be compared.

The microfluidics flow-patterning approach discussed here is utilized to form barcode-structured antibody arrays. We have demonstrated that those barcode arrays enable unique clinical applications in which a large number of proteins are assayed from very small sample sizes. For example, we utilized a microchip platform called the single-cell

barcode chip (SCBC) to perform a comprehensive functional analysis of rare cells from clinical specimens.<sup>13</sup> This chip was composed of  $\sim 1000$  separate microchambers into which single cells or small, defined cell colonies were isolated. Each microchamber contained two duplicate copies of an antibody array. We used the SCBC to profile quantitatively the levels of 12 secreted (functional) proteins from single tumor-antigen-specific T cells collected from a melanoma cancer patient responding to adoptive T cell immunotherapy.<sup>14</sup> A full functional analysis of those T-cells required co-analysis of several hundred such single cell assays, and the interpretation of the results required direct comparisons between cancer patient samples and those collected from healthy donors. This application highlights the unique combination of requirements that were fulfilled with the microfluidics flow-patterning technique. As examples, we needed a reasonably high multiplexing capacity and a 10-fold higher array density than is achievable with conventional spotted arrays. The high density is critical since each single-cell assay required 26 separate biomolecular assays to be executed within each of the 2–3 nl volume microchambers. High assay sensitivity for single cell profiling is required, implying the need for a high surface coverage of the patterned biomolecules. In addition, it was necessary to integrate several hundred measurements into a single analysis, and to directly compare data sets between patients and healthy donors. These demands required patterning uniformity over a  $\sim 6 \text{ cm}^2$  chip surface area, and low chip-to-chip variability. Finally, algorithms for digitizing the raw fluorescence data from the individual barcode stripes required a high level of pattern structure uniformity across the chip surface to aid in automated data capture and digitization. These requirements were met by using barcodes that were patterned with an optimized chemistry,<sup>15</sup> but were hand prepared by skilled researchers. This last point ultimately limits broader applications. Here we describe an integrated microfluidics/

<sup>a)</sup>Present address: The Methodist Hospital Research Institute; 6670 Bertner ST, Mail Stop R7-121, Houston TX 77030.

<sup>b)</sup>Author to whom correspondence should be addressed. Electronic mail: heath@caltech.edu.

robotics tool for automating the flow patterning technique. The tool produces barcode patterned substrates at a rate that is comparable with array spotter tools, while retaining the characteristics needed for a demanding, quantitative clinical application.

The challenges associated with automating the production of flow patterned microarrays are twofold. First, there is the problem of scale. The microarray features are initially patterned as  $\sim 0.8$  m long,  $20\ \mu\text{m}$  wide stripes of ssDNA that meander over the surface of an aminated or poly-L-lysine-coated glass microscope slide. Most applications yield improved performance as the DNA loading within a given stripe is increased,<sup>16,17</sup> and so it is important to optimize for both high and uniform loading across the entire length of these channels. The aspect ratio of each stripe ( $10^5$ – $10^6$ ), coupled with the loading requirements, places severe demands on the flow patterning chemistry. In addition, a full microarray pattern is composed of between 10 and 50 stripes, each of which represents a distinct ssDNA sequence. Thus, a robotics system must self-align a large number of injectors with a given elastomeric mold at an alignment precision of order  $100\ \mu\text{m}$ , and it must do so many times across a  $\sim 1\ \text{m}^2$  tray, in order to sequentially and automatically address many chips.

The second challenge relates to the mechanical characteristics of the elastomeric flow patterning mold. This mold is only weakly bonded to the glass surface; it is removed once the patterning process is complete. In addition, the individual stripes within a barcode are separated from one another by as little as  $20\ \mu\text{m}$ , which is the wall thickness of microchannels in the flow patterning template. Thus, the machine's injector head must mate and then disengage each elastomeric chip very gently, and the intermediate DNA injection process must be executed at low pressures to prevent both wholesale elastomer delamination and localized channel-to-channel delamination, both of which lead to chip failure.

We first give a brief overview of the robotics-driven sequential production of up to 18 flow-patterned glass slides, followed by a statistical evaluation of their quality – both in terms of feature variability on a given slide, and across different slides produced in the same run. We then use these substrates for multiplexed assays of secreted proteins from single cells, and we statistically compare data sets of single cell assays between hand-patterned and robotics-patterned slides, and between two different robotics-patterned slides.

## II. EXPERIMENTAL SECTION

### A. Robotics design

The robotics-driven flow patterning apparatus is shown in Figure 1(a). Major components of the robotics are numerically labeled in the figure, including the chip support tray (1), the injector module (2), the DNA solution reservoirs (4), and the translation motors (5). A detailed scheme of the injector module is presented in Fig. 1(b); the injector employs a standard microfluidics interfacing scheme wherein stainless steel pins are inserted into punched access holes that bridge the top surface of the PDMS, flow patterning molds with the microchannel/glass surface interfaces below.<sup>18</sup> The stainless

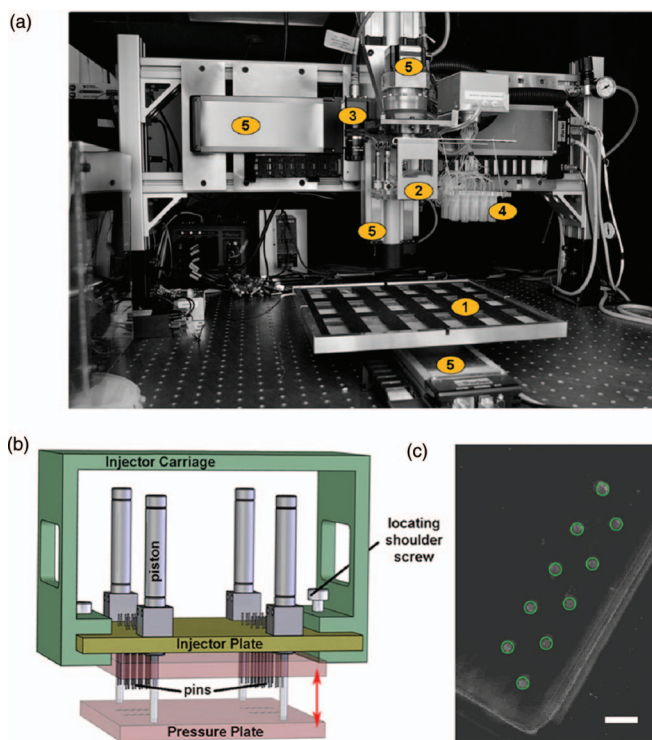


FIG. 1. (Color) The robotics platform for automated microfluidics flow patterning of glass slides. (a) An overview of the instrument as implemented. Substrates are arrayed on the slide stage (1) and thereafter are addressed sequentially by a mobile injector head (2). A camera system (3) images the substrate access holes to guide alignment as the injector interfaces each substrate, and reagents are supplied from a set of adjacent microvials (4). Mechanical motion in the  $x$ ,  $y$ ,  $z$ , and  $\theta$  axes is effected by a combination of linear stages and stepper drives (5). (b) Drawing showing detail of the injector assembly. This drawing illustrates the pin interface used to engage each substrate and the pneumatic pressure plate which prevents delamination when disengaging. (c) An image from the camera system during substrate alignment. The field of view encompasses just one corner of the substrate; green circles (enhanced for clarity) indicate access holes in the PDMS that have been recognized by the software pattern recognition algorithm and are used for fine adjustment of the injector head prior to interfacing. Scale bar: 2 mm.

steel pins are embedded within a laser-drilled acrylic “injector plate,” and are arranged according to a pre-determined pattern that matches the substrate access holes (Fig. 1(c)). This scheme allows for a high density of fluidic inputs, and it reduces substrate filling to a parallel process. However, the scheme also introduces a challenge related to the alignment of the pins to the access holes: the pins are  $650\ \mu\text{m}$  in diameter while the access holes are only  $500\ \mu\text{m}$ . The dimensional mismatch forces the elastomer to expand upon interfacing and thereby form a leak-proof seal around the pins. However, the soft nature of the elastomer also means that misalignment of the two components can lead to unwanted deformation or unintended puncturing of the PDMS, instead of smooth mating of pin and hole. The problem is compounded by the fact that all the pins must be aligned simultaneously, leaving very small tolerances for angular misalignment of the injector plate.

As such, substrate-injector alignment is done in two phases. A pre-alignment is achieved by virtue of plastic cutouts on the substrate tray, which loosely define the locations of the (up to) 18 PDMS flow patterning chips. Finer alignment is provided by a Cognex IS5400 camera system

mounted to the side of the injector head. Prior to engaging each substrate, the camera is positioned directly over the chip and images the access hole pattern, comparing it to a pre-trained image using built-in pattern recognition algorithms (Figure 1(c));  $x$ ,  $y$ , and  $\theta$  deviations are reported to the control software which adjusts the appropriate translation stages and re-images the substrate iteratively until a null deviation reading is achieved. The injector head is then shifted a pre-calibrated distance to align with the substrate and is slowly lowered into place until the pins sink 1 mm into their corresponding access holes.

Once engaged, DNA solutions are supplied to the injector head from a set of adjacent, disposable microvials via short lengths of Tygon tubing. The delivery of precisely metered, microliter scale aliquots is typically accomplished by external syringe pumps, but here we offload metering responsibility to the PDMS chips themselves. Specifically, the microfluidic channels are fabricated with a set of input access holes, but no output holes, thereby creating a closed system upon substrate engagement. Because PDMS is air permeable, a pressurized solution injected into the input ports can displace air within the microchannel until it reaches the end.<sup>18</sup> In this way, a very precise volume, defined by the input access hole and microchannel dimensions, is metered into each channel. The on-chip metering allows for a relatively simple implementation of the pressure system used to drive solutions, as depicted in Figure 2. Briefly, the solution-containing microvials are connected to a pair of three-way solenoid valves (Gems Sensors M-series) that can be configured to connect one of three inputs to the vials. The inputs establish either positive pressure, a vent, or a closed system within the vials. The latter two states are achieved by virtue of an open and a sealed input on the solenoids. The positive pressure input derives from a compressed air source which is regulated to the pressure required to drive solutions through their microfluidic channels. Typical pressures range from 2–5 psi, and are set with inverse proportion to the pattern density of the chip in order to prevent cross-contamination of solutions from adjacent channels. An electronically controlled proportional valve is integrated in the pressure line and opens gradually to introduce the pressure via a gentle ramp, thereby avoiding splashing of the solutions in their microvials. After engaging a substrate, the microvials are pressurized to drive their solutions into the microchannels. Once filling is complete, the solenoids reconfigure to vent the

microvials, and then reconfigure again to create a closed system prior to disengaging. This final state helps to balance hydrostatic pressures and prevent leaking from the injector pins in the disengaged state.

Disengaging the injector head from a substrate requires additional engineered components; because the injector pins form a tight seal with their corresponding substrate access holes, care must be exercised to prevent the PDMS mold and glass substrate from delaminating while extracting the pins. The injector plate is therefore fitted with four pneumatic pistons whose rods secure a second “pressure plate” to its underside. Matching through holes in the pressure plate enable the injector plate pins to protrude beneath it during substrate engagement and manipulation. When disengaging a substrate, this pressure plate is extended to brace the PDMS firmly against the slide tray while the pins are extracted. The entire injector/pressure plate assembly slides into a slot on the machined injector carriage and is reproducibly located via two shoulder screws. This modular implementation makes it easy to swap injector heads with different pin configurations from run to run, thereby allowing significant flexibility in substrate design.

## B. Substrate fabrication

We standardized virtually all aspects of the microfluidic flow channel chip dimensions, and streamlined their production.<sup>19,20</sup> To generate PDMS substrates, a deep reactive ion etched Si master is clamped between two machined aluminum plates; the upper plate contains cutouts that will define the substrate dimensions, and the master is positioned such that its features are aligned within these cutouts (Figure 3). The resulting dimensional uniformity, particularly in thickness, obviates the need for sophisticated depth control when interfacing the injector head with substrates; a pre-calibrated constant is sufficient. The most critical substrate features, however, are the access holes which bridge microfluidic channels with the top side of the substrate; these must be positioned very precisely and reproducibly relative to one another because the rigidly defined injector plate interfaces with them simultaneously. We therefore developed a template to mold access holes as the substrate cures. Specifically, stainless steel wires are embedded into a laser-drilled acrylic plate in the required pattern. After pouring PDMS into the alu-

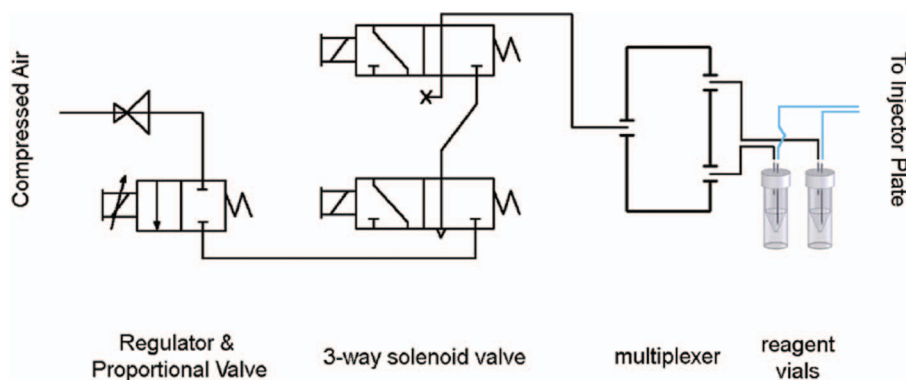


FIG. 2. (Color online) Schematic representation of the instrument's simplified pressure system for driving reagents.

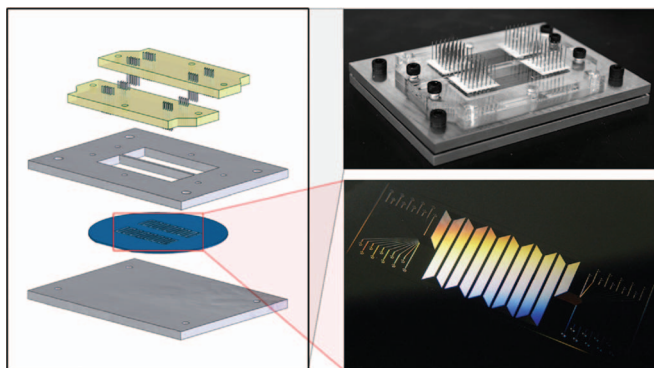


FIG. 3. (Color) The aluminum stencil used to fabricate each PDMS substrate standardizes the overall patterned dimensions and the access hole placement and size. A silicon wafer bearing barcode microfeatures is first sandwiched between two aluminum plates; PDMS precursor is poured into the cutouts and acrylic plates for molding access holes are affixed on top.

minum/silicon mold assembly (Fig. 3), this plate is secured to the top side such that the wires extend into the PDMS below. Upon curing, the plate is removed, leaving behind the templated inlet and outlet ports. The wires do not extend completely to the underlying Si mold, which prevents damage to the Si mold. Thus, a very thin membrane of PDMS at the bottom of each access hole is retained. For the inlet ports, these membranes are easily punctured in a single step by pressing the substrate onto the top side of the same acrylic plate used

to originally mold the holes. The thin membranes are retained in the outlet ports. This means that we are able to generate a dead-end filled substrate that yields extremely consistent metering volumes. The substrate also fills relatively quickly due to the high air permeability of the thin membranes at the output ports.

### C. Software and operation

The mechanical components of the instrument are controlled by custom software written in National Instruments (NI) Labwindows/CVI. Stage motion is powered by a standard 6K 4-Axis Motion Controller, while a NI DAQ card (PCI-6052E) provides digital and analog outputs to regulate an array of relays, solenoids, and proportional valves. The software presents an interface that allows users to click which of the 18 microchip positions on the substrate tray are to be processed. Once a run is initiated, the software assumes active control of all components, and processes the marked substrates sequentially without further intervention. Figure 4 illustrates the instrument's process flowchart for a typical barcoding run; from the user perspective, it simply consists of laying out the substrates in their tray, filling the microvials with DNA solutions, and loading the appropriate configuration files before pressing a button to start the run. As such, the user can pattern up to 18 barcode substrates with <1 h setup time, which is ~20-fold faster than the manual process, and

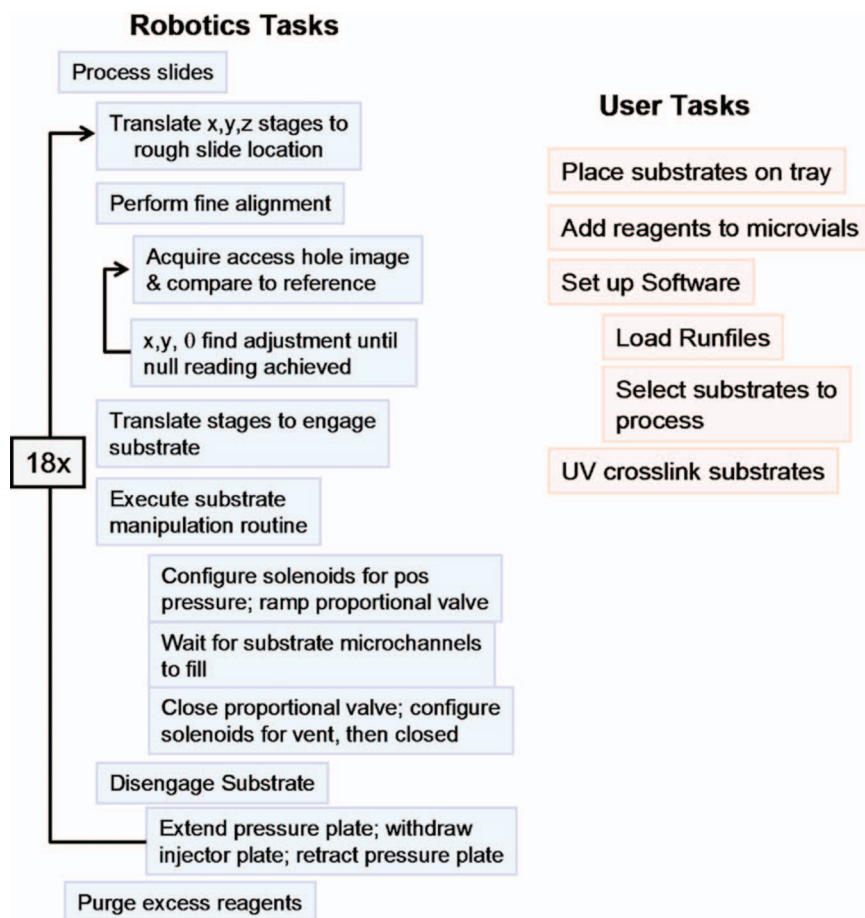


FIG. 4. (Color online) Flowchart comparing tasks required of the user and those required of the instrument to prepare a batch of barcode microarray substrates.

at least competitive with DNA spotter tools. When automated filling is complete, the microarrays are processed using the same standard protocols employed for spotted slides: after a 24 h incubation period, the slides are given a short UV exposure of  $\sim 1800$  mJ/cm<sup>2</sup> which cross links the DNA in place. Following an additional 12 h incubation, the PDMS is removed, the substrates are rinsed, and are then ready for use.<sup>21</sup>

### III. RESULTS AND DISCUSSION

We prepared a set of six 20-channel flow-patterned substrates featuring 20  $\mu\text{m}$  channels at 120  $\mu\text{m}$  pitch. For each chip, 4 adjacent microchannels were utilized to pattern 4 unique ssDNA strands, denoted by the letters A-D.<sup>22</sup> To analyze the fidelity and amount of channel-to-channel leakage that occurred during patterning, the patterned chip was characterized at two physically separate regions; 2 non-adjacent DNA stripes (A and C) were assayed at one region, while the remaining two (B and D) were assayed at the other. In this way, if DNA from channels A or C leaked into either or both of channels B or D, for example, such leakage would be detected. The DNA stripes on the first five of the substrates were investigated by first blocking with 1% Bovine Serum Albumin (BSA) and then incubating with Cy3-conjugated complementary DNA. Figure 5(a) depicts the raw signal from one of these substrates, with the separate assay regions aligned to one another. Only the intended four channels exhibit sig-

nal in a repeating fashion across the chip; the automated process did not lead to delamination of the PDMS from its glass substrate.

We quantified the fluorescence signal from each of the five barcode-patterned substrates to assay feature quality and consistency. Raw fluorescence intensities were collected for each DNA sequence at eleven locations per chip, spanning a 28 cm length of the flow channel. Figure 5(b) compares the averaged intensities for each stripe on each chip. The error bars reveal high signal uniformity across the eleven imaged regions, and the absolute signal intensities for each DNA strand are in good agreement with one another across the five chips. DNA stripes on individual chips consistently demonstrate  $<10\%$  coefficient of variation (CV), while the averaged values for each DNA across multiple chips exhibit  $<12\%$  CV (Fig. 3). These data confirm that the automated instrument is capable of generating a consistent batch of substrates, with a quality that is comparable to previously established standards for hand-made substrates.<sup>15,23</sup>

We now turn towards demonstrating the applicability of our flow patterned substrates to miniaturized bioassays via the multiplex detection of proteins secreted from single macrophage cells. The flow patterned glass slides are first incorporated into a microfluidics chip, called a SCBC, designed for the capture of single cells and small cell colonies (Figure 6). Microfluidic chip designs for cell isolation and interrogation have previously been reported, albeit with

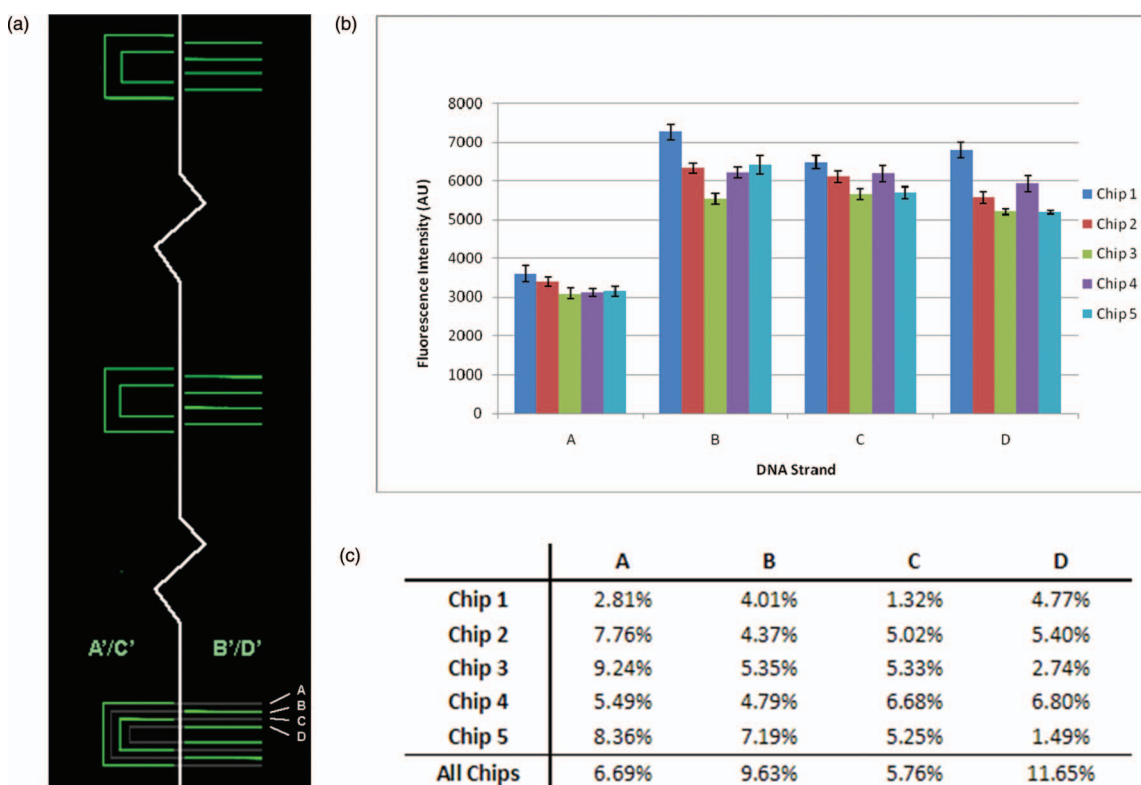


FIG. 5. (Color) Statistical analysis of DNA patterns created using the automated robotics platform. (a) Fluorescence image of a barcode microarray that is validated with alternating DNA sequences to check for unintended crosstalk or contamination. The channel morphology is overlaid on the bottom repeat; each microchannel meanders across the chip to create multiple repeats of the same pattern. (b) Average fluorescence intensities for DNA sequences A-D are quantified for five separate barcode substrates patterned by the instrument. Error bars represent the standard deviation calculated from eleven measurements per sequence. (c) Coefficients of variance (CVs) for each DNA sequence calculated from eleven regions of each chip. The averaged intensity for each sequence is then compared amongst chips and a CV is calculated to quantify chip-to-chip consistency.

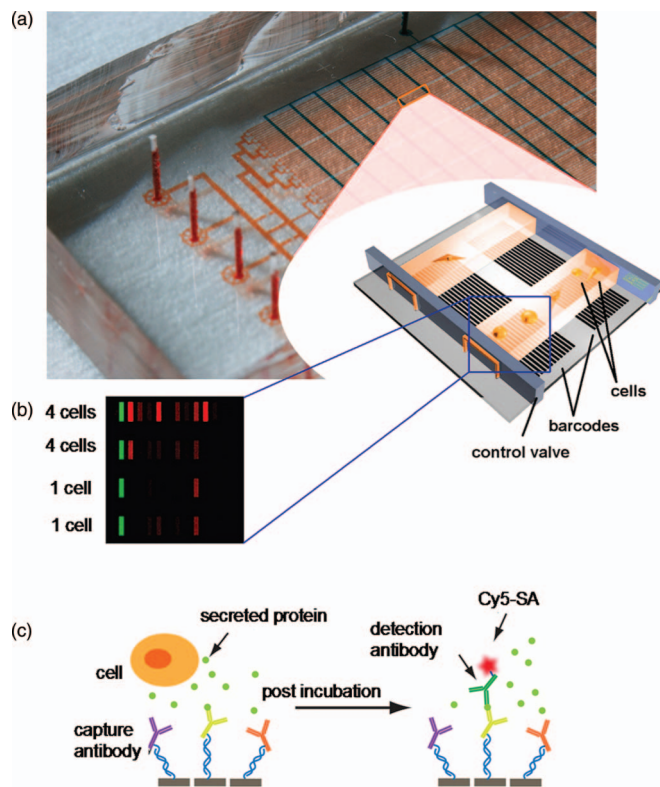


FIG. 6. (Color) The single cell barcode chip. (a) An optical micrograph of the SCBC, with a schematic inlay of two discrete chambers. (b) Raw data collected from four adjacent chambers is shown; the green bar is used for alignment registration while the red bars represent protein data. The fluorescence intensity from each of the red bars may be utilized to extract quantitative protein abundances through the use of calibration curves. (c) Representation of the sandwich-like antibody assays utilized for the SCBC measurements. Capture antibodies are arrayed onto a barcode microarray via DEAL chemistry and sequester proteins secreted from an adjacent cell. The assay is developed by flushing with detection antibodies and a fluorescent reporter to form an ELISA-like sandwich.

different detection schemes.<sup>24,25</sup> Here, the DNA microarrays are converted into antibody microarrays using a cocktail of DNA-labeled capture antibodies. This is the DNA-encoded antibody library, or DEAL, technique.<sup>17</sup> Cells are then introduced and isolated into any of approximately 1000 separate 3 nl volume microchambers on the SCBC. The numbers of cells in a given chamber are recorded; of the 1000 such experiments on a single chip, typically 100–200 are single-cell experiments, while the remaining are 0-cell, 2-cell, 3-cell, etc., experiments (Fig. 6(b)). The chip is then incubated for a period of time during which the captured cells secrete proteins that are selectively captured by the antibody barcodes. The cells are then washed from the chip and a cocktail of detection antibodies and fluorescent dye labels are added to develop the protein assays (Figs. 6(b) and 6(c)). The measured fluorescence levels from the individual feature stripes are digitized and then compared against calibration curves<sup>22</sup> to provide an estimate of the numbers of protein molecules detected, which, in turn, yields information on the sensitivity of the robotics-patterned antibody microarrays. By comparing the statistics of protein secretion levels from single cells assayed on one chip with identical assays from a second chip, the chip-to-chip variability can be assessed. A related SCBC,

but designed for assaying phosphorylated membrane and cytoplasm proteins from single, lysed cancer cells, has recently been reported by us.<sup>15</sup> That chip utilized hand-made microarray patterns, and only permitted  $\sim 120$  single- and few-cell experiments per chip, but was otherwise similar in concept to the chip described here.

The DNA microarrays utilized for this demonstration were derived from 20-element patterning microfluidics. Twelve of the elements were used for the bioassay, and each contained one of 12 unique DNA sequences, A–M,<sup>22</sup> flow-patterned with a stripe width of 20  $\mu\text{m}$  and at a 50  $\mu\text{m}$  pitch. Two substrates from a batch of four were carried forward for the cell assays; the patterning PDMS was removed and the new microfluidic device (Fig. 6(a)) was bonded in its place. Eleven of the DNA stripes were converted to form an antibody array, with antibodies chosen to correspond to secreted proteins. They included: monocyte chemoattractant protein (MCP)-1, interleukin (IL)-6, granulocyte macrophage colony stimulating factor (GM-CSF), macrophage migration inhibitory factor (MIF), interferon (IFN)- $\gamma$ , vascular endothelial growth factor (VEGF), IL-10, IL-8, matrix metalloproteinase (MMP)-9, and tumor necrosis factor (TNF)- $\alpha$ , and IL-2. IL-2 is not expected to be secreted from macrophage cells, and so serves as a negative control. The remaining DNA stripe provides an alignment reference for the final read-out. Once the antibody array is assembled, the cells were prepared for loading. We investigated the human monocyte cell line, THP-1. These cells were first differentiated into the macrophage lineage using phorbol 12-myristate 13-acetate (PMA) and stimulated with lipopolysaccharide (LPS);<sup>26</sup> the PMA elicits a morphological change in the THP-1 cells (Figure S2), and LPS activates the toll-like receptor-4 on the cell surface,<sup>27</sup> emulating the response of macrophages to gram negative bacteria. The stimulated cells are then loaded, as a dilute suspension, into a set of 80 microchannels that span the length of the flow patterned glass slide. A set of 14 integrated valves<sup>18</sup> is activated to divide the microchannels into 1040 discrete microchambers, each containing single or small numbers of cells (Fig. 6(a)). Each chamber is examined to record the number of cells it contains, and the entire platform is then placed in a CO<sub>2</sub> incubator at 37 °C for 24 h while secreted proteins are captured onto the antibody microarray. Afterwards, the cells are flushed from the microchannels, and the protein assays are developed with a cocktail of biotinylated secondary antibodies followed by the addition of streptavidin-Cy5 fluorophores. The fluorescence intensities are digitized through the use of an Axon GenePix 4400A array scanner, coupled with custom written image processing routines. The resulting data is a table that lists, for each microchamber, the numbers of cells in that microchamber and the digitized fluorescence for each of the assayed proteins and for the DNA alignment reference stripe.

We quantified our raw data by first establishing a signal baseline. For each protein assayed, we averaged the raw signal values across all the individual chambers which contained single cells. Using the averaged signal recorded from the IL-2 assay stripes as the noise level, we calculated the signal-to-noise (ratio) (S/N) for each protein, and set a threshold of  $S/N \geq 4$  to signify positive detection of a protein. By that standard,

nine proteins were identified (S/N levels are in parentheses after the protein names): IL-6 (4), INF- $\gamma$  (14), GMCSF (27), VEGF (89), IL-10 (190), MMP9 (498), IL-8 (560), TNF- $\alpha$  (566), and MIF (1504). Comparisons against separately generated calibration curves<sup>22</sup> revealed limits of detection that were similar to or slightly worse than commercial enzyme-linked immunosorbent assays (ELISAs). For example, VEGF yielded 3 pg/mL vs 2.5 pg/ml and IL-8 yielded 75 pg/mL versus 25 pg/mL.

Full biological analysis of the single cell secretome data is provided in Ref. 28; here we simply provide analysis of the data in order to validate the microarray and chip technology. Figure 6(b) depicts a set of four adjacent chambers, two of which contained single cells and two of which contained four cells each. We grouped the data according to numbers of cells per microchamber. The data within each group was then sorted according to the level of MIF secretion. Error bars are plotted for many of the data points; these are derived from chambers that contained two copies of the 20-element barcode and thereby yielded replicate measurements from which measurement error could be estimated. The plot of Fig. 7(a) clearly demonstrates a cumulative effect in the observed signal, as increasing numbers of cells yields a greater proportion of chambers with high signal levels. The maximum signal level for each of the shown set of experiments is near saturation and so does not increase with increasing numbers of cells. Note that a percentage of the  $n = 1, 2,$  and 3 cell chambers

yield MIF signal levels that are similar to those observed for the 0-cell chambers: 52% (1 cell), 37% (2 cell), 22% (3 cell). These values consistently indicate that between 50% and 60% of the individual macrophage cells secrete low levels of MIF, but they also indicate that the 1, 2, and 3 cell data sets represent sets of measurements that are distinct from each other, and distinct from the 0-cell data. There was no correlation between the level of secreted protein and the location of the associated microchamber on the chip surface.

A heat map of protein secretion levels for the single cell experiments is provided in Figure 7(b). This data demonstrates the stochastic nature of protein secretion at the single cell level. These single cell fluctuations, for a given protein level, can be compared between two chips as a means of comparing the chip-to-chip variability. While any given microchamber may yield a very different result from another microchamber, a statistically significant measurement of the single cell fluctuations, as recorded on one chip, should be indistinguishable from those recorded on a second chip. Such a comparison is provided in Figure 7(c) between data sets collected from two different chips, and both the average protein level, and the detailed distributions, are chip-independent. Similar analyses were also done for the proteins MMP9 ( $p = 0.640$ ) and TNF- $\alpha$  ( $p = 0.435$ );<sup>22</sup> among the remaining proteins, only IL-8 and IL-10 fail to yield  $p$ -values above 0.1. Of these two proteins, time-studies (not presented here) indicate that the secretion of IL-10 is delayed relative to

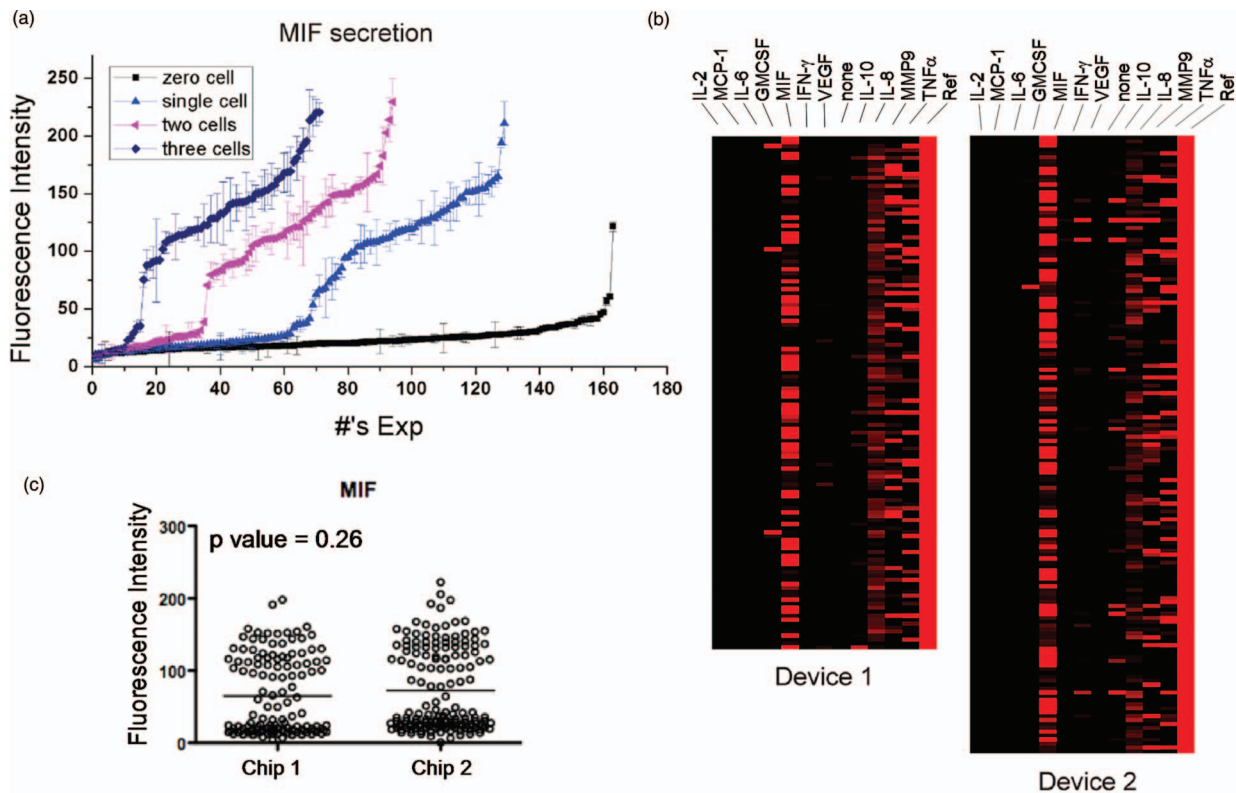


FIG. 7. (Color) Multiplex protein assays from single LPS-stimulated macrophage cells. (a) The distribution of MIF secretion for chambers containing between zero and three cells is plotted. Chambers with more cells exhibit a greater proportion of elevated signals, implying a cumulative effect. Error bars represent standard deviations that are calculated from barcode repeats within individual chambers. (b) Heat maps depicting protein secretion for chambers with single cells on each of two chips. (c) Scatter plots of MIF secretion in single cell chambers illustrate the distribution of secretion profiles; the horizontal line represents the average of all the individual measurements. The  $p$  value descriptor implies that the two sets of data from different chips are statistically indistinguishable.

the other proteins, and so longer time studies would likely increase the chip-to-chip p-values for this protein. IL-8, while secreted early, is also characterized by  $\sim 10\times$  higher background signal, and so is intrinsically a less reliable measurement than the other detected proteins. The results indicate a high level of consistency across both a single microchip, and across multiple chips. This means that data taken from different chips can be seamlessly integrated to increase sampling statistics, or that data from one set of cells can be compared against that taken from a different set of cells with confidence.

#### IV. CONCLUSIONS

Traditional DNA microarray technology is an exceedingly useful tool, thanks in part to the development of significant infrastructure dedicated to microarray production and processing. As the applications of microarrays continue to evolve, there is a push towards further miniaturization.<sup>8,11,29</sup> Microfluidic flow patterning, as described here, will not likely extend to below 5–10  $\mu\text{m}$  feature sizes. However, it provides an attractive combination of multiplexing (up to 50 using the platform described here), miniaturization, reproducibility, sensitivity, cost, and throughput. This combination of characteristics makes it enabling for several exciting fundamental and clinical applications ranging from single cell proteomics<sup>13,15,28</sup> to high resolution tissue engineering.<sup>30</sup>

#### ACKNOWLEDGMENTS

This work was supported by the National Cancer Institute (Grant No. 1U54CA151819–01 (JRH PI)), the Grand Duchy of Luxembourg via a subcontract from the Institute for Systems Biology, and the Jean Perkins Foundation. We acknowledge Mike Roy for many useful discussions regarding instrument design. K.H. acknowledges support from a Samsung Foundation Fellowship.

<sup>1</sup>D. Rose, *Microfluidic Technologies and Instrumentation for Printing DNA Microarrays* (Eaton Publishing Co., Natick, 2000), pp. 19–38.

<sup>2</sup>R. S. Kane, S. Takayama, E. Ostuni, D. E. Ingber, and G. M. Whitesides, *Biomaterials* **20**, 2363 (1999).

<sup>3</sup>E. Delamarche, A. Bernard, H. Schmid, B. Michel, and H. Biebuyck, *Science* **276**, 779 (1997).

<sup>4</sup>C.-E. Ho, C.-C. Chieng, M.-H. Chen, and F.-G. Tseng, *J. Microelectromech. Syst.* **17**, 309 (2008).

<sup>5</sup>D. A. Chang-Yen, D. G. Myszka, and B. K. Gale, *J. Microelectromech. Syst.* **15**, 1145 (2006).

<sup>6</sup>D. J. Lockhart, H. Dong, M. C. Byrne, M. T. Follettie, M. V. Gallo, M. S. Chee, M. Mittmann, C. Wang, M. Kobayashi, H. Norton, and E. L. Brown, *Nat. Biotechnol.* **14**, 1675 (1996).

<sup>7</sup>S. Singh-Gasson, R. D. Green, Y. Yue, C. Nelson, F. Blattner, M. R. Sussman, and F. Cerrina, *Nat. Biotechnol.* **17**, 974 (1999).

<sup>8</sup>K. Salaita, Y. H. Wang, and C. A. Mirkin, *Nat. Nanotechnol.* **2**, 145 (2007).

<sup>9</sup>S. A. Lange, V. Benes, D. P. Kern, J. K. H. Hörber, and A. Bernard, *Anal. Chem.* **76**, 1641 (2004).

<sup>10</sup>M. Geissler, E. Roy, J.-S. Deneault, M. Arbour, G. A. Diaz-Quijada, A. Nantel, and T. Veres, *Small* **5**, 2514 (2009).

<sup>11</sup>I. Barbulovic-Nad, M. Lucente, Y. Sun, M. Zhang, A. R. Wheeler, and M. Bussmann, *Crit. Rev. Biotechnol.* **26**, 237 (2006).

<sup>12</sup>G. C. Tseng, M.-K. Oh, L. Rohlin, J. C. Liao, and W. H. Wong, *Nucleic Acids Res.* **29**, 2549 (2001).

<sup>13</sup>C. Ma, R. Fan, H. Ahmad, Q. Shi, B. Comin-Anduix, T. Chodon, R. C. Koya, C. Liu, G. A. Kwong, C. G. Radu, A. Ribas, and J. R. Heath, *Nat. Med.* **17**, 738 (2011).

<sup>14</sup>R. A. Morgan, M. E. Dudley, J. R. Wunderlich, M. S. Hughes, J. C. Yang, R. M. Sherry, R. E. Royal, S. L. Topalian, U. S. Kammula, N. P. Restifo, Z. Zheng, A. Nahvi, C. R. de Vries, L. J. Rogers-Freezer, S. A. Mavroukakis, and S. A. Rosenberg, *Science* **314**, 126 (2006).

<sup>15</sup>Y. S. Shin, H. Ahmad, Q. Shi, H. Kim, T. A. Pascal, R. Fan, W. A. Goddard III, and J. R. Heath, *ChemPhysChem* **11**, 3063 (2010).

<sup>16</sup>D. S. Dandy, P. Wu, and D. W. Granger, *Proc. Natl. Acad. Sci. U.S.A.* **104**, 8223 (2007).

<sup>17</sup>R. C. Bailey, G. A. Kwong, C. G. Radu, O. N. Witte, and J. R. Heath, *J. Am. Chem. Soc.* **129**, 1959 (2007).

<sup>18</sup>J. Melin and S. R. Quake, *Annu. Rev. Biophys. Biomol. Struct.* **36**, 213 (2007).

<sup>19</sup>A. M. Christensen, D. A. Chang-Yen, and B. K. Gale, *J. Micromech. Microeng.* **15**, 928 (2005).

<sup>20</sup>C. M. Klapperich, *Expert Rev. Med. Devices* **6**, 211 (2009).

<sup>21</sup>H. Y. Wang, R. L. Malek, A. E. Kwitek, A. S. Greene, T. V. Luu, B. Behbahani, B. Frank, J. Quackenbush, and N. H. Lee, *Genome Biol.* **4**, Art# R5 (2003).

<sup>22</sup>See supplementary material at <http://dx.doi.org/10.1063/1.3636077> for a listing of oligonucleotide reagents used in the assays, calibration curves for multiplex protein assays, morphological changes in THP-1 cells following exposure to PMA/LPS, and scatter plots for selected proteins from different SCBC chip experiments.

<sup>23</sup>J. Wang, H. Ahmad, C. Ma, Q. Shi, O. Vermesh, U. Vermesh, and J. R. Heath, *Lab Chip* **10**, 3157 (2010).

<sup>24</sup>E. M. Bradshaw, S. C. Kent, V. Tripuraneni, T. Orban, H. L. Ploegh, D. A. Haffler, and J. C. Love, *Clin. Immunol.* **129**, 10 (2008).

<sup>25</sup>H. Zhu, G. Stybayeva, J. Silangeruz, J. Yan, E. Ramanculov, S. Dandekar, M. D. George, and A. Revzin, *Anal. Chem.* **81**, 8150 (2009).

<sup>26</sup>C. D. Dumitru, J. D. Ceci, C. Tsatsanis, D. Kontoyiannis, K. Stamatakis, J. H. Lin, C. Patriotis, N. A. Jenkins, N. G. Copeland, G. Kollias, and P. N. Tsichlis, *Cell* **103**, 1071 (2000).

<sup>27</sup>A. Aderem and R. J. Ulevitch, *Nature (London)* **406**, 782 (2000).

<sup>28</sup>Y. S. Shin, F. Remacle, R. Fan, K. Huang, W. Wei, H. Ahmad, R. D. Levine, and J. R. Heath, *Biophys. J.* **100**, 2378 (2011).

<sup>29</sup>J.-U. Park, M. Hardy, S. J. Kang, K. Barton, K. Adair, D. K. Mukhopadhyay, C. Y. Lee, M. S. Strano, A. G. Alleyne, J. G. Georgiadis, P. M. Ferreira, and J. A. Rogers, *Nature Mater.* **6**, 782 (2007).

<sup>30</sup>U. Vermesh, O. Vermesh, C. Ma, G. A. Kwong, K. Hwang, and J. R. Heath, *Angew. Chem., Int. Ed.* **50**, 7378 (2011).